CHALLENGES OF NANOMEASUREMENTS AND COMPLEX CHARACTERIZATION OF IRON OXIDE NANOPARTICLES

Štefan Luby[1], Peter Švec[1], Monika Benkovičová[1], Matej Jergel[1], Milan Timko[2]

[1] Institute of Physics, Slovak Acad. Sci., Dúbravská cesta 9, 845 11 Bratislava, Slovakia,
[2]Institute of Exp. Physics, Watsonova 47, 040 01 Košice, Slovakia
E-mail: stefan.luby@savba.sk

Received 30 April 2017; accepted 05 May 2017

1. Introduction

Nanoscience and nanotechnology (N&N) introduced a way of building structures by bottom-up approach which provides numerous opportunities in the field of new materials, medicine and information technology. An intrinsic part of N&N is nanometrology. It is characterized by the effort for reproducibility of data and responsibility of researchers triggered by a huge diversity of nanostructures. They fill the space between big molecules at one side and micro- and bulk materials at the other side. It is impossible to scrutinize and check all data published by the growing number of standard and open-access journals that benefit from investments flowing into the nano-research [1,2]. As *pars pro toto* let us mention the flagship project *Graphen*e of European Union supported by 1 bil. € (2013 – 2033) [3].

In nanometrology attention is paid to all physical quantities. Nevertheless, most important are structure, morphology, composition and porosity of nanostructures. They are studied by 25 - 30 methods divided into two basic groups [4,5]:

• EAA (ensemble-averaging approach), where we analyse larger samples by AES, SIMS, XPS, XRD, DSC, TGA, DLS, BET, etc.

• IPA (individual particle approach), which give information about small samples. Examples are AFM, HR TEM, SEM, STM but also nanoSQUIDs challenging the single molecular or atomic spin [6].

Examples of nanostructures are graphene and silicene (2D), nanotubes, nanowires (1D), nanoparticles (NPs), nanodots (0D) [7] (Fig. 1). Our choice in this paper are spherical nanoparticles from iron oxide family with good ability to self-assemble. Their complex characterization is based upon DSC-TGA, SEM, TEM, XRD and SQUID data.

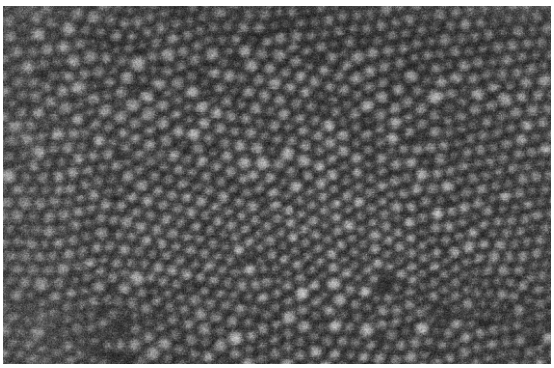

Fig. 1: *SEM picture of a quite regular γ-Fe_2O_3 (6.4 nm) NP array deposited onto oxidized Si by means of a modified Langmuir-Schafer technique [7]. Particles are separated by surfactant capping.*

2. Iron oxide family

Iron oxide NPs are studied for nearly half a century. They have a central position particularly in magnetic NP research as shown by numerous reviews, e.g. [8-10]. This is due to their biocompatibility and low toxicity in the human body and good magnetic properties. NPs are used in recording and data storage, ferrofluids, in cancer therapy and diagnostics (theranostics), magnetic resonance imaging, sensors and biosensors, catalysis, tissue repair, etc. Eight iron oxide phases have been recognized. Among them hematite, maghemite and magnetite are frequently used (Tab. 1).

Tab. 1. *Basic properties of main iron oxide family members [8,10]*.

Property	Magnetite	Maghemite	Hematite
Formula	Fe_3O_4	γ-Fe_2O_3	α-Fe_2O_3
Density [g/cm^3]	5.18	4.87	5.26
Melting point [^{o}C]	1583 – 1597	1566	1350
Crystall. system	cubic	cubic/tetrahedral	rhombohed./ hexag.
Free energy of form. [kJ/mol]	–742.7	–1012.6	–711.1
Conductivity type	n, p	n	n
Energy gap [eV]	0.1	2.0	2.3
Magnetism	ferro	ferri	weak ferro*
Curie temp. [K]	850	820 – 986	956
Sat. magnetization [emu/g]	92 – 100	60 – 80	0.3

*antiferromagnetic under 260 K – Morin temperature.

A group of pivotal importace are γ-Fe_2O_3 superparamagnetic iron oxide NPs with applications in material research and medicine. They transform to α phase between 200 and 500 ^{o}C, whereas bulk samples transform between 500 and 600 ^{o}C [11]. Therefore an important property of NPs is their thermal stability. For example transformation temperature T_T is the limiting working temperature of gas sensors of exhaust gases, for fire detection, etc.

3. Preparation, thermal stability and transformation of γ-Fe_2O_3 nanoparticles

Our Fe_3O_4/γ-Fe_2O_3 NPs are prepared as colloidal solution from (Fe(acac)3 with 1.2-hexadecanediol, oleic acid and oleyl amine (surfactant) in phenyl ether at 200 ^{o}C/30 min plus 265 ^{o}C/30 min heating. After centrifugation and removal of excessive surfactant they are redispersed in toluene. This master solution is stored at 5 ^{o}C. The core diameter of NPs is 6.4±0.6 nm, surfactant is 1 nm thick [7]. When exposed to air Fe_3O_4 is slowly oxidizing to γ-Fe_2O_3 even at room temperature (RT) [11]. In parallel with pure γ-Fe_2O_3 NPs we studied their mixtures with Pd NPs (6 – 7 nm, covered by oleylamine, purchased from PlasmaChem). The idea was to modify transformation and electrical conductivity of arrays. The samples were prepared by casting γ-Fe_2O_3 colloidal solution or its pre-calculated mixtures with Pd NPs solution onto Si substrates. Fe_2O_3/Pd 100/1, 100/5 and 100/10 mixed samples were investigated (ratios relate to NPs).

Thermal stability was studied by XRD at the isochronal annealings in air (1 h) between 500 ^{o}C to 770 ^{o}C. In pure Fe_2O_3 samples maghemite (m) phase persisted up to 550 ^{o}C (Fig. 2) and mixed m + h (hematite) phase was recorded at 600 ^{o}C. In the Pd containing samples T_T is shifted about 100 ^{o}C downward to 500 ^{o}C for both 100/1 and 100/5 mixtures (Fig. 2). The high T_T of γ-Fe_2O_3 NPs is an advantage in sensors technology. We assume that γ phase is stabilized (at the NPs size from 5 to 30 nm) by the surface free energy [12]. For comparison in [13] 8 – 20 nm γ-Fe_2O_3 nanoparticles showed the transition to α phase already at 481 ^{o}C.

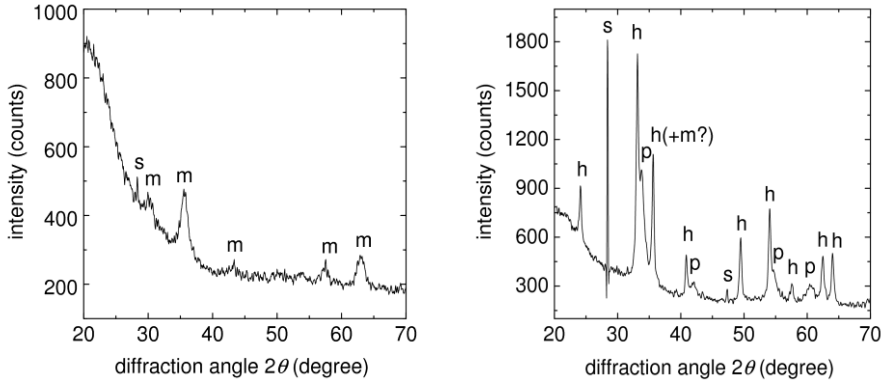

Fig. 2: *XRD pattern of (left) Fe_2O_3 sample annealed at 550 ^oC/1 h (m – maghemite, s – substrate) and (right) Fe_2O_3/Pd 100/1 sample annealed at 500 ^oC/1 h (h – hematite, p – palladinite, s - substrate) [13].*

Our NPs are crystalline already *in statu nascendi*, as it was documented by both XRD and TEM/STEM (Fig. 3). This is not surprising because in our NPs the distance from interior to the surface is short and defects diffuse out to annihilate at the surface.

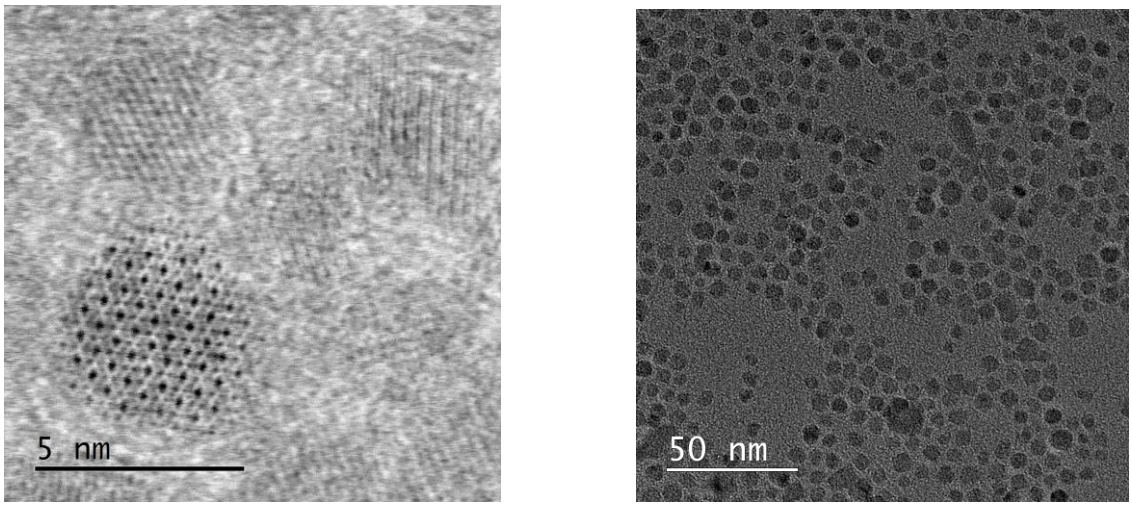

Fig. 3: *STEM bright field micrograph with [110] viewing direction of Fe_3O_4 (left). At the right side TEM picture of Fe_2O_3 NP clusters on Cu grid covered by holey carbon is shown.*

4. DSC – TGA measurements

Differential scanning calorimetry and thermal gravimetry were done with Fe_2O_3 NP solutions in Al_2O_3 crucibles using heating rate of 10 K/min in Ar ambient. (The chamber is not oxygen proof.) Previous DSC spectra have shown ageing of NPs in solution with chloroform which is used for fast transfer of NPs onto water surface in Langmuir-Schaefer deposition technique because it evaporates fast. However, it contains chlorine which can react with surfactant. Therefore we switched to toluene (Fig. 4). Analyses were repeated after 14 days and 5 weeks. The stability improved but the ageing at combined RT/frigidaire conditions was still observed. In DSC spectra an exothermic peak was found at 550 K. We identify it as the removal of surfactant. The corresponding weight loss was recorded by TGA. Two additional exothermic peaks, sometimes split, were found at higher temperatures. They are not accompanied by weight loss. We assume that peaks at 700 – 760 K are related to the

final crystallization of iron oxide NPs. The crystallization normally develops up to 0.80 – 0.85 T_m (melting temperature) [14]. Features around 800 K are related to γ → α transformation of pure γ-Fe_2O_3 which is finished at 870 K, complying to about 600 ^oC from XRD measurements (Fig. 2). Pd shifts these peaks to lower temperatures as it was also confirmed by DSC. As expected, with increasing heating rate the DSC spectra are moved to higher temperatures and *vice versa*. The heating rate of 10 K/min is from the point of γ → α transformation an equivalent of the static heating. The decrease of T_T due to Pd content could be explained by diffusion of Pd into iron oxide NPs, where nuclei for the formation of α phase originate. In conclusion, DSC – TGA studies correspond to XRD measurements of transformation temperatures of our samples.

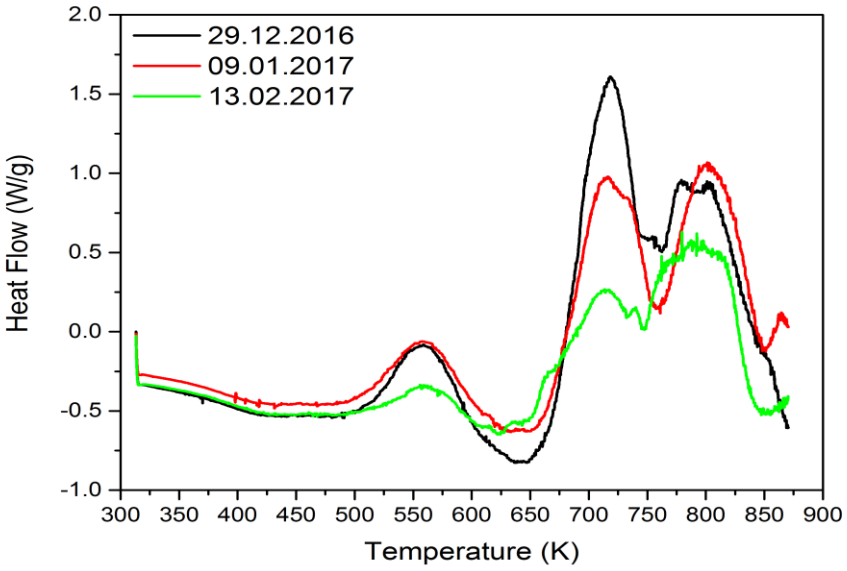

Fig. 4: *DSC spectra of the NPs solution in toluene.*

5. Magnetic measurements

Iron oxide NPs consist of a single magnetic domain below the critical size of 15 nm. They are also superparamannetic which means that at RT the thermal energy overcomes anisotropy energy barrier and the cooperative phenomenon of ferromagnetism is not observed [10,15]. Particles are important for biomedical applications, because they do not retain any magnetism after removal of the external field [15]. On the other hand under blocking temperature T_B they are magnetically ordered. In this work we have studied magnetization vs field dependencies. T_B was measured using ZFC - FC approach [10] at 100 Oe. The samples were analysed by SQUID. Due to our very small samples the diamagnetic contribution of Si substrate should be considered. Here we will show only the data for Fe_2O_3 related to γ → α transformation. In Fig. 5 arbitrary values are shown. Afterwards the data were calibrated by measuring the sample mass. The calibrated results are given in Tab. 2. From the following Tab. 3 a tendency of increase of M_s with increasing NPs size is obvious. Therefore the magnetization of our small particles is surprisingly high. (The value 80.6 emu/g seems, however, unrealistic, because the bulk value shoud be 76 emu/g [16].) High M_s might be ascribed to the preparation at high temperatures.

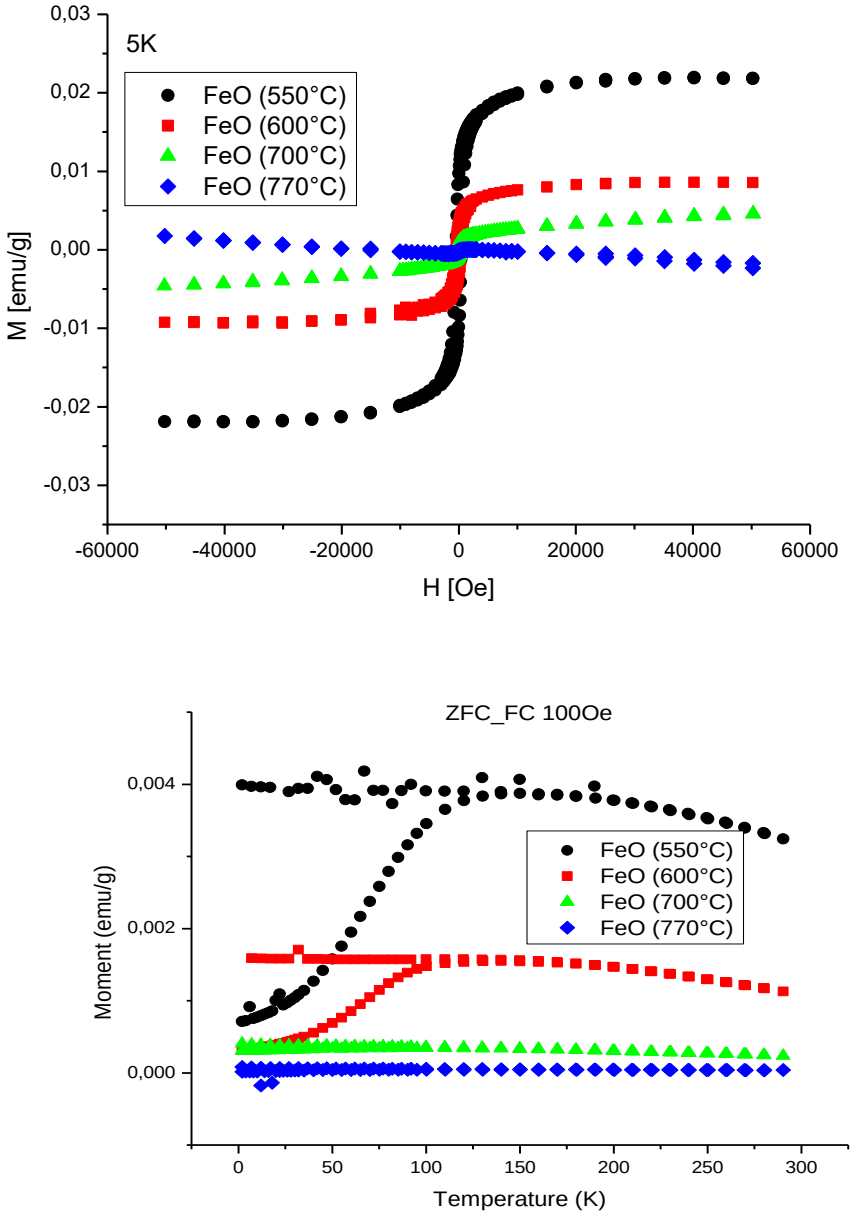

Fig. 5: *M – H dependences of γ-Fe_2O_3 NPs at 5 K (top) and ZFC – FC measurements of T_B (bottom) with γ-Fe_2O_3 NPs annealed between 550 and 770 °C.*

Tab. 2. *Calibrated saturation magnetization M_s data of Fe_2O_3 NPs at 50 kOe and their blocking temperatures.*

Sample	Heating [°C]	T_B [K]	M_s [emu/g] at 5 K	M_s [emu/g] at 300 K
Fe_2O_3	no	50	80,6	62.5
Fe_2O_3	550	125	61.9	61.9
Fe_2O_3	600	125	25.9	21.6
Fe_2O_3	700	100	13.5	6.0
Fe_2O_3	770	125	-5.8	1.6
Si subsrate	no		-2.3	-9.2

Tab. 3. *Saturation magnetization M_s vs size of iron oxide NPs [16].*

Method	d [nm]	M_s [emu/g]
thermal decomposition	28 - 37	8 - 67
calcination	30	74
ultrasonic decomposition	25	38 - 55
hydrothermal	12 - 26	53 - 73
solvothermal	12	26 - 42
coprecipitation	10	69.8
high-temperature solution reaction	6.4 ± 0.6	62.5
	bulk	76

6. Conclusion

We have presented a complex study of the thermal stability and γ → α transformation of iron oxide nanoparticle arrays. The complementary techniques of XRD, TEM, STEM, DSC-TGA and SQUID provided a coherent picture of our structures with the aim to follow the present efforts towards the reproducibility and reliability in the nanotechnology. The results were applied in the fabrication of sensitive gas sensors of NO_2 and acetone [17].

Acknowledgement

The authors would like to thank M. Kotlár for TEM analyses and D. Kostiuk for technical assistance. This work was financially supported by the grants of Slovak Research and Development Agency No. APVV-14-0891 and Scientific Grant Agency of the Ministry of Education of Slovak Republic and the Slovak Academy of Sciences No. VEGA-2/0010/2015 as well as by CNR – SAS 2016 – 2018 common programme.

References:

[1] D. Lowe: http://blogs.sciencemag.org/pipeline/archives/2016/05/26/ visited 02. 2017.
[2] Editorial: *Nature Nanotech.*, **9**, 94 (2014).
[3] EC 2013, http://graphene-flagship.eu/project 03. 2017.
[4] Nanotechnology and Human Health, I. Malsch, C. Edmond (eds.). CRC Press, Boca Raton, USA (2014), ISBN 978-0-8493-8144-7.
[5] Metrology and Standardization for Nanotechnology, E. Mansfield et al. (eds.) Wiley – VCH, Weinheim, Germany (2017), ISBN 978-3-527-34039-2.
[6] C. Granata et al.: *Eur. Phys. J. B*, **86,** 272 (2013).
[7] S. Luby: Nanosvet na dlani, CVTI SR, VEDA, vyd. SAV, Bratislava (2016), ISBN 978-80-224-1548-4.
[8] A. S. Teja, P.-Y. Koh: *Prog. Cryst. Growth&Charact. Mater*. **55**, 22 (2009).
[9] G. Kandasamy, D. Maity: *Int. J. Pharmaceutics* **496**, 191 (2015).
[10] W. Wu et al.: *Sci. Technol. Adv. Mater.* **16,** 023501 (2015).
[11] J. Ivanco et al.*: Sensor Lett.*, **11**, 2322 (2013).
[12] N. Randrianantoandro et al.: *Mater. Lett***.,** **47**, 150, (2001).
[13] R. Ch. Biswal: *Sens. Actuators B* **157**, 183 (2011).
[14] N. Okui: *Polymer* **31**, 92 (1990),
[15] A. K. Gupta, M. Gupta: *Biomaterials*, **26**, 3995 (2005).
[16] D. Cao et al.: *Sci. Rep*. **6**, 32360, 9 p.
[17] S. Capone et al. : *Sens. Actuators B* **243**, 895 (2017).